Contemporary Mathematics

Recent Progress in the Stochastic Analysis of Turbulent Mixing

Wurigen Bo, Baolian Cheng, Jian Du, Brian Fix, Erwin George, James Glimm, John W. Grove, Xicheng Jia, Hyeonseong Jin, Hyunsun Lee, Yuanhua Li, Xiaolin Li, Xinfeng Liu, David H. Sharp, Lingling Wu, and Yan Yu

Abstract. We outline a program for the study of turbulent mixing of compressible fluids. We emphasize recent progress and steps still to be taken.

1. Introduction

We are interested in the description of fluid mixing layers which grow out of acceleration driven instabilities, including the classical cases of Rayleigh-Taylor (RT) instability, driven by a steady acceleration and Richtmyer-Meshkov (RM) instability, driven by an impulsive acceleration. Classical references to this subject, which has attracted a high level of interest over many decades, include [**1, 24**]; more recent references can be traced from the series [**11**], and earlier volumes in this series.

Our program starts with high resolution methods of numerical simulation of two (or more) distinct fluids, continues with analytic analysis of these solutions, and the derivation of averaged equations. All steps are to be compared with available experimental data and the final step of averaged equations is compared as well with the direct simulation of the of the microfluid equations describing the fluid mixture.

In summary, the steps are as follows:

(1) High resolution methods for simulation of fluid flow with discontinuities and steep gradients with comparison to other numerical methods [**13**].

B. Cheng, J. W. Grove and D. H. Sharp were supported by the U.S. Department of Energy.

J. Glimm, J. Du, B. Fix and X. Liu were supported in part by the NSF Grant DMS-0102480.

J. Glimm, W. Bo, B. Fix, X. Jia, H. Lee, X. Li, Y. Li, L. Wu, and Y. Yu were supported in part by the Army Research office Grant W911NF0510413 and the U.S. Department of Energy Grant DE-FG02-90ER25084.

J. Glimm was supported in part by the U.S. Department of Energy Grant DE-AC02-98CH10886.

J. Glimm, H. Lee and Y. Yu were supported in part by the Los Alamos National Laboratory Contract 1481600105.

X. Li, Y. Li and X. Liu were supported in part by U.S. Department of Energy Grant DEFC02-01ER25461.

(2) Direct numerical simulation (DNS) of the microphysical equations of fluid mixing, with validation through comparison to laboratory experiments [**15, 16**].
(3) Derivation of averaged equations and closure hypotheses for fluid mixing [**2, 3, 17, 9**].
(4) Mathematical analysis of properties of fluid mixing and of the averaged equations [**4, 5, 6, 8**].
(5) Validation of closure hypotheses and the averaged equations by comparison to data from microphysical simulations [**20**].

Each of these steps will be explained in a section of this paper.

2. Front Tracking

We emphasize three new developments for the Front Tracking code FronTier.

2.1. Local Grid Based Tracking. In grid free tracking, the tracked front is a triangulated surface, propagating freely through a rectangular volume filling mesh. In grid based tracking, the front is regularized, or reconstructed, at each time step. After propagation, the points of intersection of the front with all grid cell edges are determined. Assuming at most one such intersection for each grid cell edge, the complete interface is reconstructed in a simple manner from these intersections.

Grid based tracking is very robust. (It is similar to the level set in this sense, and both are derived from computer science graphics routines). However, grid based tracking is inaccurate, as is the level set method. Grid based tracking, the level set, and untracked simulations, which also determine an interface from grid based information, all have a form of interface smoothing which resembles surface tension. We call this property numerical surface tension, for reasons which will become clear in the next section.

Local grid based tracking [**13**] combines these two algorithms, preserving the advantages of each. This algorithm relies on the more accurate grid free tracking unless there is a bifurcation. This part of the algorithm is robust as the problems with the grid free propagation occur only with bifurcations of the interface. When a bifurcation occurs, a small box is constructed around it. Grid based propagation is used inside the box. The grid free surface triangulation near the box has to be rejoined to the reconstructed grid inside the box in a construction which also has a grid based flavor.

The result is favorable: the accuracy of grid free tracking and the robustness of grid based tracking are both preserved.

We carried out a systematic study [**13**] of this new algorithm in comparison to other interface methods (level sets, volume of fluids), and found that locally grid based front tracking is the best of all methods tested. An extract from this study is presented in Fig. 1.

2.2. Surface Tension and Physical Mass Diffusion. Front Tracking is a very convenient framework to add additional surface based physics. Normal vectors and curvature tensors are supported by the code.

Surface tension forces a pressure jump at the interface proportional to the surface curvature. Within the normal propagation step for the dynamic time step of the front, there is a solution of a Riemann problem. This Riemann problem

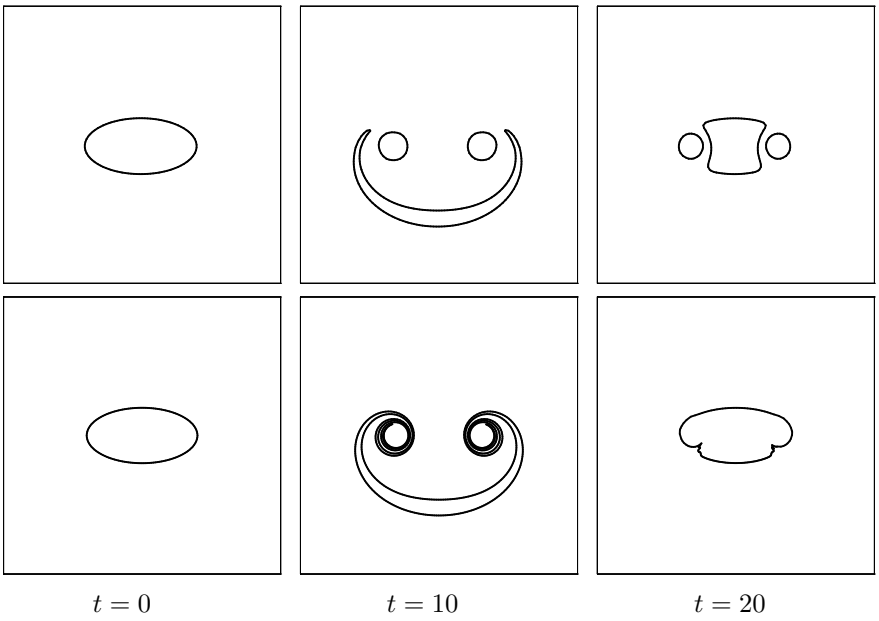

FIGURE 1. Comparison between level set and front tracking on velocity reversal. The upper sequence shows the results of level set using fifth order WENO while the lower sequence shows the results of front tracking using the fourth order Runge-Kutta for the point propagation. The ellipse at time $t = 0$ is placed in a dipole velocity field. The velocity is reversed at t = 10, so any deviation between the first and third columns is a numerical error.

is central to Front Tracking, as it connects dynamically the states on the two sides of the front; it replaces a finite difference operation across the front. In the Riemann solution, the basic equations are equilibration of the normal velocity and the pressure at the front. On this basis, one solves for the mid state pressure [**10**]. In the presence of surface tension, with a specified jump in the pressures (proportional to the surface curvature at the point), the equation of pressure equilibration is modified due to the pressure jump. But an equation for the equilibration of the two mid state pressures is still valid, and is used after modification in the usual manner in the solution for the mid state pressures and for the Riemann problem.

To compute with physical mass diffusion, two steps are needed. First, and most difficult, is to eliminate numerical mass diffusion. Front Tracking does this very effectively. High order or spectral compact differential schemes may also accomplish this goal. The second step is to add limited amounts of mass diffusion back into the calculation, on the basis of prescribed values for the physical mass diffusion constant. Our algorithm for doing this is based on the following ideas:

(1) Determine the density jump $\rho_r - \rho_l$ or mass fraction jump at the current time by taking the values at the edges of a suitable finite difference stencil.
(2) Record as a history variable the amount of mass which has diffused through the interface (and remains within the stencil size).

Experiment Simulation	Comment	α
Read-Youngs	Immiscible [**22**] # 33	0.066
FronTier	Immiscible	0.062
Smeeton-Youngs	Miscible [**25**] # 112	0.062
FronTier	Miscible	0.070
TVD	Ideal Untracked [**14**]	0.035
FronTier	Ideal	0.09

TABLE 1. Mixing rates compared: FronTier simulation compared to experiment and contrasted to untracked (TVD) and ideal fluid FronTier simulations.

(3) Use the density jump, the diffused mass and the diffusion constant to compute (from an analytic solution of the diffusion in 1D, i.e. with spectral accuracy) the amount of mass to be diffused in the current time step.

2.3. FronTier-Lite. We have extracted from the FronTier code developed by the authors and colleagues over a period of years the purely geometrical parts (physics independent parts) of front tracking. This code is modular and can be called as an external library in other codes. We have released this code for public distribution. See

`http://www.ams.sunysb.edu/FTdownload`

3. Simulations of Rayleigh-Taylor Instabilities

We report on a new series to Rayleigh-Taylor mixing simulations based on the improved algorithms described in Sec. 2.1 and the improved physics modeling described in Sec. 2.2. The results for the immiscible simulations (surface tension) are presented in [**15**], and the results for miscible simulations (physical mass diffusion) will be presented in a future paper. Here we compare simulation and experiment in terms of the growth rate of the bubble side of the mixing layer, defined by the dimensionless constant α in the equation

$$h = \alpha A g t^2 \tag{3.1}$$

for the bubble (light fluid) penetration h in terms of the Atwood number A, gravity g and time t.

The values of $\alpha = \alpha_b$ are given in Table 1. We also compare simulation to experiment using another measures of the mixing process, defining an α_r associated with the bubble radius. See Table 2.

4. Averaged Equations and Closure

Two-phase flow equations are derived by applying an average process to the microscopic dynamics. Let the function X_k be the phase indicator for material k ($k = 1, 2$); *i.e.*, $X_k(t, \mathbf{x})$ equals 1 if position $\mathbf{x}$ is in fluid k at time t, zero otherwise. We average the advection law for the indicator function X_k of the region occupied by the fluid k,

$$\frac{\partial X_k}{\partial t} + v_{\text{int}} \cdot \nabla X_k = 0 \ . \tag{4.1}$$

Data/Comment	α_b	α_r
Smeeton & Youngs [**25**]	0.067	0.01
Cheng *et al.* [**8**]		
Average #104, 105, 114		
RNG Fixed Point [**8**]	0.06	0.01
FronTier immiscible	0.062	0.01

TABLE 2. Comparison of bubble radius and of height fluctuations between experimental data, theory and simulation.

It was shown [**12**] that X_k satisfies (4.1). Here $v_{\rm int}$ is the microphysical velocity evaluated at the interface (the velocity component normal to the boundary ∂X_k is continuous so that $v_{\rm int}\dot{\nabla}X_k$ is well defined). We also average the microscopic conservation equations

$$\frac{\partial \rho}{\partial t} + \nabla \cdot \rho \mathbf{v} = 0 \ , \tag{4.2}$$

$$\frac{\partial \rho \mathbf{v}}{\partial t} + \nabla \cdot \rho \mathbf{v}\mathbf{v} = -\nabla p + \rho g \ , \tag{4.3}$$

$$\frac{\partial \rho E}{\partial t} + \nabla \cdot \rho \mathbf{v} E = -\nabla \cdot p\mathbf{v} + \rho \mathbf{v} g \ . \tag{4.4}$$

Here the dependent variables $\mathbf{v}$, ρ, p, and E denote, respectively, the velocity, density, pressure, and total energy with $E = e + \mathbf{v}^2/2$ and e the internal energy.

Scale breaking physics such as mass diffusion or surface tension will add new terms to these equations. The extension of these equations, including their closure has been extended to arbitrary n fluids in the incompressible case [**9**].

4.1. Averaged Equations. We denoted the ensemble average $\langle\cdot\rangle$. The average $\langle X_k\rangle$ of the indicator function X_k is denoted β_k; $\beta_k(z,t)$ is then the expected fraction of the horizontal layer at height z that is occupied by fluid k at time t. The quantities ρ_k and p_k are, respectively, phase averages of the density ρ and pressure p:

$$\rho_k = \frac{\langle X_k \rho\rangle}{\langle X_k\rangle} \ , \quad p_k = \frac{\langle X_k p\rangle}{\langle X_k\rangle} \ . \tag{4.5}$$

The quantities v_k and E_k are phase mass-weighted averages of the fluid z-velocity v_z and total energy E:

$$v_k = \frac{\langle X_k \rho v_z\rangle}{\langle X_k \rho\rangle} \ , \quad E_k = \frac{\langle X_k \rho E\rangle}{\langle X_k \rho\rangle} \ . \tag{4.6}$$

Applying the ensemble average to Eqs. (4.1)-(4.4), we obtain the one-dimensional two-pressure two-phase flow averaged equations. Let $s = 0, 1, 2$ for planar, cylindrical or spherical geometry. We follow [**12, 2, 3, 23**] to obtain

$$\frac{\partial \beta_k}{\partial t} + \langle \mathbf{v} \cdot \nabla X_k\rangle = 0 \ , \tag{4.7}$$

$$\frac{\partial (\beta_k \rho_k)}{\partial t} + \frac{1}{z^s}\frac{\partial}{\partial z}(z^s \beta_k \rho_k v_k) = 0 \ , \tag{4.8}$$

$$\frac{\partial(\beta_k\rho_k v_k)}{\partial t} + \frac{1}{z^s}\frac{\partial}{\partial z}(z^s\beta_k\rho_k v_k^2) + \frac{\partial(\beta_k p_k)}{\partial z} = \left\langle p\frac{\partial X_k}{\partial z}\right\rangle + \beta_k\rho_k g \ , \tag{4.9}$$

$$\frac{\partial(\beta_k\rho_k E_k)}{\partial t} + \frac{1}{z^s}\frac{\partial}{\partial z}\left[z^s\beta_k v_k(\rho_k E_k + p_k)\right] = \langle p\mathbf{v}\cdot\nabla X_k\rangle + \beta_k\rho_k v_k g \tag{4.10}$$

for the volume fraction β_k, velocity v_k, density ρ_k, pressure p_k, and total energy E_k of phase k. Here $k = 1 = b$ (bubble) and $k = 2 = s$ (spike) denote the light and heavy fluids respectively, $k' = 3 - k$ and $g = g(t) > 0$ is the gravity.

Three interfacial terms are defined by

$$\langle \mathbf{v}\cdot\nabla X_k\rangle = v^*\frac{\partial\beta_k}{\partial z} \ , \tag{4.11}$$

$$\left\langle p\frac{\partial X_k}{\partial z}\right\rangle = p^*\frac{\partial\beta_k}{\partial z} \ , \tag{4.12}$$

$$\langle p\mathbf{v}\cdot\nabla X_k\rangle = (pv)^*\frac{\partial\beta_k}{\partial z} \ . \tag{4.13}$$

We have thus defined

$$v^* = \frac{\langle \mathbf{v}\cdot\nabla X_k\rangle}{\langle \mathbf{n}_3\cdot\nabla X_k\rangle} \ , \quad p^* = \frac{\langle p\mathbf{n}_3\cdot\nabla X_k\rangle}{\langle \mathbf{n}_3\cdot\nabla X_k\rangle} \ , \quad (pv)^* = \frac{\langle p\mathbf{v}\cdot\nabla X_k\rangle}{\langle \mathbf{n}_3\cdot\nabla X_k\rangle} \ , \tag{4.14}$$

where $\mathbf{n}_3$ is the unit normal vector in z direction. The quantities q^*, $q = v,\ p,\ pv$, represent averages of microscopic quantities.

The gradient ∇R of the Reynolds stress $R = \langle\rho\mathbf{v}\mathbf{v}\rangle - \langle\rho\mathbf{v}\rangle^2 / \langle\rho\rangle$ does not appear in (4.9) and a related second moment is absent from each of the equations (4.10). An exact identity [**2, 3, 7**] expresses R as a sum of first order two phase products expressing velocity fluctuations between phases and two pure phase R_k Reynolds stress terms, reflecting within phase velocity fluctuations. Specifically,

$$R = \beta_1\beta_2\frac{\rho_1\rho_2}{\langle\rho\rangle}(v_1 - v_2)^2 + \beta_1 R_1 + \beta_2 R_2 \ . \tag{4.15}$$

The first term in (4.15) is the between-phase Reynolds stress and the last two terms are the within-phase Reynolds stresses. For the problems we are interested in, it appears that the within-phase velocity fluctuations and turbulence are small, and we have chosen to set R_k to zero.

4.2. The v^* closure. In [**17**] the interface velocity v^* has been derived exactly from (4.7) and (4.8) independently of any closure assumption. The result is extended to the present context ($s = 0, 1, 2$) in the following theorem.

THEOREM 4.1. *The interface quantity v^* has the exact formula*

$$\begin{aligned} v^* &= \frac{\beta_1\left[\dfrac{\partial(z^s v_1)}{\partial z} + \dfrac{z^s}{\rho_1}\dfrac{D_1\rho_1}{Dt}\right]v_2 + \beta_2\left[\dfrac{\partial(z^s v_2)}{\partial z} + \dfrac{z^s}{\rho_2}\dfrac{D_2\rho_2}{Dt}\right]v_1}{\beta_1\left[\dfrac{\partial(z^s v_1)}{\partial z} + \dfrac{z^s}{\rho_1}\dfrac{D_1\rho_1}{Dt}\right] + \beta_2\left[\dfrac{\partial(z^s v_2)}{\partial z} + \dfrac{z^s}{\rho_2}\dfrac{D_2\rho_2}{Dt}\right]} \\ &\equiv \mu_1^v v_2 + \mu_2^v v_1 \ , \end{aligned} \tag{4.16}$$

where the mixing coefficients have the fractional linear form

$$\mu_k^v = \frac{\beta_k}{\beta_k + d_k^v\beta_{k'}} \ . \tag{4.17}$$

The constitutive factor d_k^v is also expressed in the exact form

$$d_k^v(z,t) = \frac{\dfrac{\partial(z^s v_{k'})}{\partial z} + \dfrac{z^s}{\rho_{k'}}\dfrac{D_{k'}\rho_{k'}}{Dt}}{\dfrac{\partial(z^s v_k)}{\partial z} + \dfrac{z^s}{\rho_k}\dfrac{D_k\rho_k}{Dt}} \ . \tag{4.18}$$

The factor $d_k^v(z,t)$ in (4.18) is a ratio of logarithmic rates of volume creation for the two phases.

A closure condition of spatial homogeneity assumes

$$d_k^v(t) = \frac{\displaystyle\int_{Z_k}^{Z_{k'}} \frac{\partial(z^s v_{k'})}{\partial z} + \frac{z^s}{\rho_{k'}}\frac{D_{k'}\rho_{k'}}{Dt}\,dz}{\displaystyle\int_{Z_k}^{Z_{k'}} \frac{\partial(z^s v_k)}{\partial z} + \frac{z^s}{\rho_k}\frac{D_k\rho_k}{Dt}\,dz} = \frac{Z_{k'}^s V_{k'} - Z_k^s v_{k'}(Z_k) + \displaystyle\int_{Z_k}^{Z_{k'}} \frac{z^s}{\rho_{k'}}\frac{D_{k'}\rho_{k'}}{Dt}\,dz}{-Z_k^s V_k + Z_{k'}^s v_k(Z_{k'}) + \displaystyle\int_{Z_k}^{Z_{k'}} \frac{z^s}{\rho_k}\frac{D_k\rho_k}{Dt}\,dz} \ . \tag{4.19}$$

The identity (4.19) states that the relative extent of volume creation for the two fluid species is independent of the spatial location in the mixing zone. Thus we see that the closure (4.19) is logically and physically independent of and distinct from (4.18). Given the mixing zone edge positions $Z_k(t)$ or velocities $V_k(t) = \dot{Z}_k$, the identity (4.19) is a zero parameter model for the constitutive law $d_k^v(t)$. The boundary data $v_k(Z_{k'})$, $k = 1, 2$, are found by solving Eq. (4.8) for v_1 in the single phase region, assuming the boundary conditions (no flow at the top, $z^{+\infty}$) at the outer edges of a finite container containing the mixing layer. We also use the identity

$$Z_{k'}^s v_k(Z_{k'}) - Z_k^s v_{k'}(Z_k) = \int_{Z_k}^{Z_{k'}} \frac{\partial(z^s \overline{v})}{\partial z}\ dz = -\int_{Z_k}^{Z_{k'}} \frac{z^s\beta_k}{\rho_k}\frac{D_k\rho_k}{Dt} + \frac{z^s\beta_{k'}}{\rho_{k'}}\frac{D_{k'}\rho_{k'}}{Dt}\,dz \tag{4.20}$$

derived from (4.8) independently of closure assumptions. Thus we have

$$d_1^v(t) = \frac{Z_2^s V_2 - \displaystyle\int_{Z_1}^{z^{+\infty}} \frac{z^s\beta_1}{\rho_1}\frac{D_1\rho_1}{Dt}dz + \int_{z^{-\infty}}^{Z_2} \frac{z^s\beta_1}{\rho_2}\frac{D_2\rho_2}{Dt}dz}{-Z_1^s V_1 + \displaystyle\int_{Z_1}^{z^{+\infty}} \frac{z^s}{\rho_1}\frac{D_1\rho_1}{Dt}dz} \ , \tag{4.21}$$

We assume $(-1)^k V_k = (-1)^k \dot{Z}_k \geq 0$ so that mixing zone is expanding. The growing mixing zone entrains pure phase fluid into the mixture, and thus creates mixed fluid volume for both phases. In the incompressible case, this is seen clearly from the closed form solution

$$d_k^v(t) = \left(\frac{Z_{k'}}{Z_k}\right)^s \left|\frac{V_{k'}}{V_k}\right| \ . \tag{4.22}$$

Since we are assuming no mass transfer between the fluids, the creation of volume does not arise from interchange of mass or volume between the fluids, but rather from the entrainment of previously unmixed (pure phase fluid) into the mixing zone (this effect gives rise to the V_k terms in (4.21)) and also from the relative compression of the two fluids (a result of the logarithmic substantive derivative terms in (4.21)).

The ratio (4.19) satisfies the relation $d_1^v(t)d_2^v(t) = 1$ which is equivalent to $\mu_1^v + \mu_2^v = 1$. Furthermore, $d_k^v(t) \geq 0$ if and only if μ_k^v is nonnegative finite for $0 \leq \beta_k \leq 1$.

The p^* closure is presented in [**20**].

5. Mathematical Analysis of Mixing

A bubble merger model assumes propagation of the bubbles of light fluid into the ambient heavy fluid at the edge of the mixing zone due to combined effects of single bubble motion, added motion due to bubble interaction, and added motion due to systematic removal of the slower bubbles from the ensemble. This model predicts the Rayleigh-Taylor mixing rate correctly and additionally predicts the average bubble width and the fluctuations in the bubble heights [**8**]. These values all agree with experiment.

We have reformulated the buoyancy drag equation and corrected errors in some published versions of this equation. The equation computes the motion of the edges $Z_k(t)$ of the RT or RM mixing zone on the basis of buoyancy and phenomenological added mass and drag,

$$(\rho_k + \kappa_k \rho_{k'})\ddot{Z}_k(t) = (\rho_k - \rho_{k'})g - (-1)^k \frac{C_k \rho_{k'}(V_k - v_{k'})^2}{L_k} \ . \tag{5.1}$$

Here κ_k is an added mass coefficient due to the existence of fluid k', C_k is the drag coefficient, $v_{k'}$ is the velocity of fluid k' at the mixing zone edge Z_k, and the length scale L_k is the ratio of the structure's total volume to frontal surface area. The choice $L_\kappa^{-1} = \partial\beta_1/\partial z$ is convenient in the context of the averaged equations of §4. In fact, the equations of §4 are incomplete at the edges of the mixing zones, where a count of characteristics shows a missing equation associated with the incoming acoustic wave of the vanishing phase from the side of the single phase region. This missing information is supplied by (5.1). The added mass coefficient κ_k depends on the bubble geometry. It equals 1 for a cylindrical front bubble and 1/2 for a spherical front bubble in three space dimensions [**4, 21**]. The drag coefficient for the bubbles is fit to the growth rate for the bubble merger model, and the drag coefficient is predicted in terms of this by a further theoretical model. Both are then compared to all experimental data, including both RT and RM data, with good agreement [**4**]. The below leading order large time asymptotic expansion has been obtained as well [**6**].

The low compressibility limit of the averaged equations (Sec. 4) has been analyzed asymptotically through second order in the Mach number. Each term in the expansion is a function of z, t, and remarkably the series terms can be computed in closed form to give a mathematically exact answer [**19, 17**], going beyond the earlier closed form solution for the incompressible equations.

6. Validation of Closure Hypotheses and the Averaged Equations

The solutions of the averaged equations, obtained numerically [**18**] have been compared to the weakly compressible asymptotic solution, obtained analytically as a closed form expression [**19, 17**].

Here we present work in progress on the direct validation of the closures v^*, etc., based on analysis of the simulation data described in Sec. 3. From this study, we select data describing three dimensional Rayleigh-Taylor mixing in the nearly

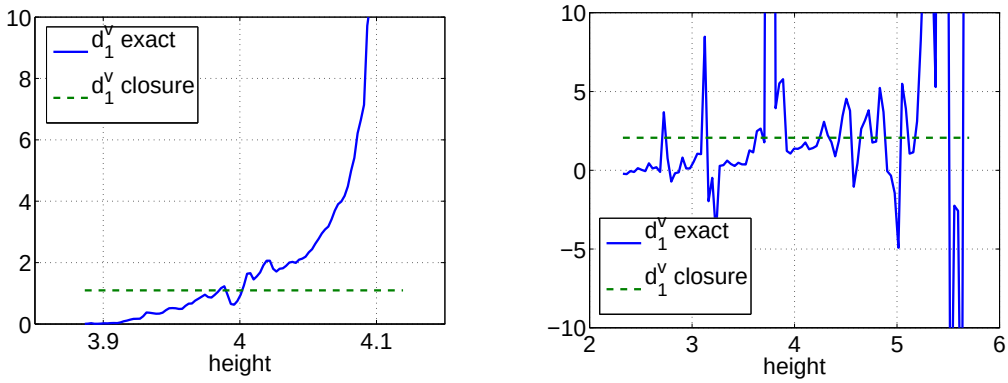

FIGURE 2. Comparison of the exact and closed ratio d_1^v. Left: $t = 3$. Right: $t = 15$.

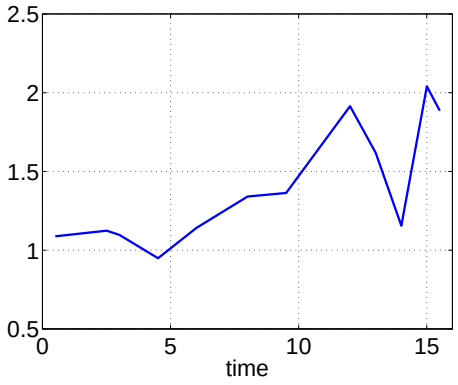

FIGURE 3. Closed constitutive law d_1^v as defined by the low compressibility ideal RT simulation data, plotted *vs.* time.

incompressible limit, with ideal flow conditions (no physical mass diffusion and no surface tension) [**16**]. The data has been analyzed for the purpose of studying the closure hypotheses of §4, specifically as related to the definition of v^* and $v^*\partial\beta_k/\partial z$. We select a typical early and typical late time $t = 3, 15$ for detailed analysis. First we compare the plots of the exact and the closed constitutive factors $d_1^v(z,t)$ and $d_1^v(t)$ for these times in Fig. 2.

The closed d_i^v, defined in terms of the simulated data, which is a function of time only, is plotted in Fig. 3.

The result of this definition of the v^* closure is presented in Fig. 4, in which we compare the exact and the closed expressions for $v_1^*\partial\beta_1/\partial z$ and the quantity $-\partial\beta_1(z,t)/\partial t$, equal to these two according to Eqs. (4.7) and (4.11).

All of this might appear overly complex for a robust multiphase flow model. We observe that for moderate Atwood numbers, the heavy and light fluids should behave in a nearly interchangeable manner, leading to $d_1^v \approx 1$. The closure $d_k^v = 1$ was originally proposed [**3**], and later set aside due to errors observed for large values

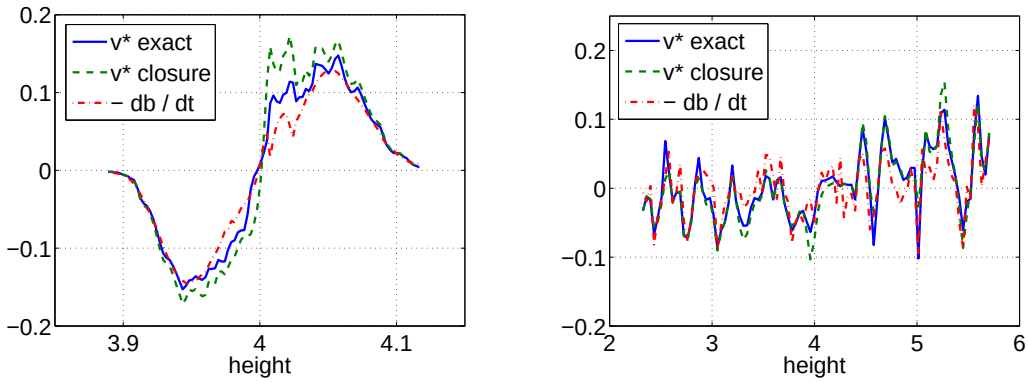

FIGURE 4. Comparison closed and exact quantities representing $v^*\partial\beta(z,t)/\partial z$. Left: $t = 3$. Right: $t = 15$.

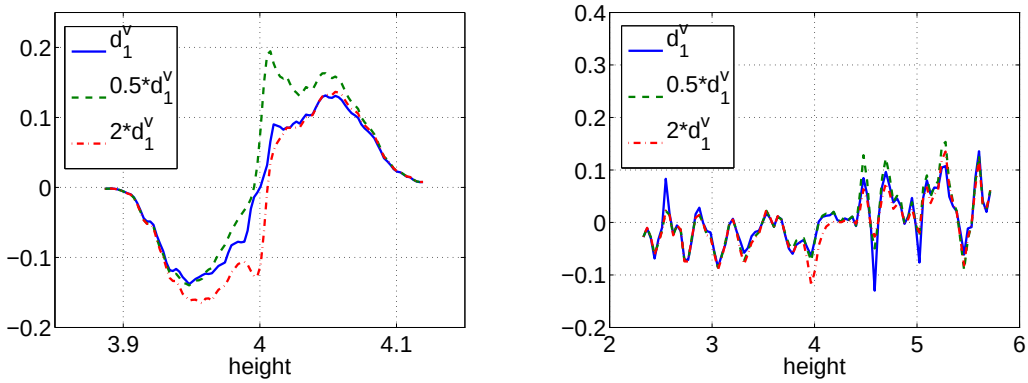

FIGURE 5. Sensitivity of $v^*\partial\beta(z,t)/\partial z$ to changes in the closed expression d_1^v up or down by factors of 2. Left: $t = 3$. Right: $t = 15$.

of A. Thus we explore the sensitivity of v^* to the definition of d_1^v, by increasing and decreasing d_1^v by factors of 2. The result shows very little change in the closed expression for $v^*\partial\beta(z,t)/\partial z$. See Fig. 5.

We observe that while the exact and to some extent the closed expressions of d_1^v, which involve numerical derivatives of simulated quantities, are noisy, the closed value satisfies the expected relation $d_1^v \approx 1$, and the term in which this closure is used in remarkably insensitive to changes in d_1^v. This fact suggests a robustness in the closed equations, a topic to which we will return in a later paper.

References

[1] S. CHANDRASEKHAR, *Hydrodynamic and Hydromagnetic Stability*, Oxford University Press, Oxford, 1961.

[2] Y. CHEN, *Two Phase Flow Analysis of Turbulent Mixing in the Rayleigh-Taylor Instability*, PhD thesis, University at Stony Brook, 1995.

[3] Y. Chen, J. Glimm, D. H. Sharp, and Q. Zhang, *A two-phase flow model of the Rayleigh-Taylor mixing zone*, Phys. Fluids, 8 (1996), pp. 816–825.
[4] B. Cheng, J. Glimm, and D. H. Sharp, *Density dependence of Rayleigh-Taylor and Richtmyer-Meshkov mixing fronts*, Phys. Lett. A, 268 (2000), pp. 366–374.
[5] ———, *A 3-D RNG bubble merger model for Rayleigh-Taylor mixing*, Chaos, 12 (2002), pp. 267–274.
[6] ———, *Dynamical evolution of the Rayleigh-Taylor and Richtmyer-Meshkov mixing fronts*, Phys. Rev. E, 66 (2002), pp. 1–7. Paper No. 036312.
[7] ———, *Multi-temperature multiphase flow model*, ZAMP, 53 (2002), pp. 2i1–238.
[8] ———, *A three-dimensional renormalization group bubble merger model for Rayleigh-Taylor mixing*, Chaos, 12 (2002), pp. 267–274.
[9] B. Cheng, J. Glimm, D. H. Sharp, and Y. Yu, *A multiphase flow model for the unstable mixing of layered incompressible materials*, Phys. of Fluids, 17 (2005). Paper No. 087102. In Press. LANL Preprint Number LA-UR-05-0078. Stony Brook University Preprint Number SUNYSB-AMS-05-01.
[10] A. Chorin and J. Marsden, *A Mathematical Introduction to Fluid Mechnics*, Springer Verlag, New York–Heidelberg–Berlin, 2000.
[11] S. B. Dalziel, ed., *Proceedings of the 9th International Workshop on the Physics of compressible turbulent mixing*, Cambridge, England, 2004.
[12] D. A. Drew, *Mathematical modeling of two-phase flow*, Ann. Rev. Fluid Mech., 15 (1983), pp. 261–291.
[13] J. Du, B. Fix, J. Glimm, X. Li, Y. Li, and L. Wu, *A simple package for front tracking*, J. Comp. Phys., (2005). In press. Stony Brook University preprint SUNYSB-AMS-05-02.
[14] E. George and J. Glimm, *Self similarity of Rayleigh-Taylor mixing rates*, Phys. Fluids, 17 (2005), pp. 054101–1–054101–13. Stony Brook University Preprint number SUNYSB-AMS-04-05.
[15] E. George, J. Glimm, X. L. Li, Y. H. Li, and X. F. Liu, *The influence of scale breaking phenomena on turbulent mixing rates*, Phys. Rev. Lett., (2005). Submitted. Stony Brook University Preprint number SUNYSB-AMS-05-11.
[16] E. George, J. Glimm, and X. F. Liu, *Turbulent mixing with physical mass diffusion*, Phys. Rev. E, (2005). Submitted. Stony Brook University Preprint number SUNYSB-AMS-05-17.
[17] J. Glimm and H. Jin, *An asymptotic analysis of two-phase fluid mixing*, Bol. Soc. Bras. Mat., 32 (2001), pp. 213–236.
[18] J. Glimm, H. Jin, M. Laforest, F. Tangerman, and Y. Zhang, *A two pressure numerical model of two fluid mixing*, SIAM J. Multiscale Model. Simul., 1 (2003), pp. 458–484.
[19] H. Jin, *The Incompressible Limit of Compressible Multiphase Flow Equations*, PhD thesis, SUNY at Stony Brook, 2001.
[20] H. Jin, J. Glimm, and D. H. Sharp, *Two-pressure two-phase flow models*, Appl. Math. Lett., (2005). Submitted. Stony Brook University Preprint number SUNYSB-AMS-05-zz and Los Alamos National Laboratory LAUR Number LA-UR-05-xxx.
[21] H. Lamb, *Hydrodynamics*, Dover, New York, 1932.
[22] K. I. Read, *Experimental investigation of turbulent mixing by Rayleigh-Taylor instability*, Physica D, 12 (1984), pp. 45–58.
[23] D. Saltz and D. Sendersky, *Computation of two-phase mixing properties in Rayleigh-Taylor instability*, tech. report, University at Stony Brook, 1999.
[24] D. H. Sharp, *An overview of Rayleigh-Taylor instability*, Physica D, 12 (1984), pp. 3–18.
[25] V. S. Smeeton and D. L. Youngs, *Experimental investigation of turbulent mixing by Rayleigh-Taylor instability (part 3)*, AWE Report Number 0 35/87, 1987.

Department of Applied Mathematics and Statistics, State University of New York at Stony Brook, Stony Brook NY 11794-3600
E-mail address: bowrg@ams.sunysb.edu

Los Alamos National Laboratory, Los Alamos, NM 87545
E-mail address: bcheng@lanl.gov

Department of Applied Mathematics and Statistics, State University of New York at Stony Brook, Stony Brook NY 11794-3600
E-mail address: jidu@ams.sunysb.edu

Department of Applied Mathematics and Statistics, State University of New York at Stony Brook, Stony Brook NY 11794-3600
E-mail address: bfix@ams.sunysb.edu

Department of Applied Mathematics and Statistics, State University of New York at Stony Brook, Stony Brook NY 11794-3600
E-mail address: egeorge@ams.sunysb.edu

Department of Applied Mathematics and Statistics, State University of New York at Stony Brook, Stony Brook NY 11794-3600, or, Center for Data Intensive Computing, Brookhaven National Laboratory, Upton NY 11973

Los Alamos National Laboratory, Los Alamos, NM 87545
E-mail address: jgrove@lanl.gov

Department of Applied Mathematics and Statistics, State University of New York at Stony Brook, Stony Brook NY 11794-3600
E-mail address: xcjia@ams.sunysb.edu

Department of Mathematics and Information, Research Institute for Basic Sciences, Cheju National University, Jeju, 690-756, Korea
E-mail address: hjin@cheju.ac.kr

Department of Applied Mathematics and Statistics, State University of New York at Stony Brook, Stony Brook NY 11794-3600
E-mail address: hslee@ams.sunysb.edu

Department of Applied Mathematics and Statistics, State University of New York at Stony Brook, Stony Brook NY 11794-3600
E-mail address: yuali@ams.sunysb.edu

Department of Applied Mathematics and Statistics, State University of New York at Stony Brook, Stony Brook NY 11794-3600
E-mail address: linli@ams.sunysb.edu

Department of Applied Mathematics and Statistics, State University of New York at Stony Brook, Stony Brook NY 11794-3600
E-mail address: xfliu77@ams.sunysb.edu

Los Alamos National Laboratory, Los Alamos, NM 87545
E-mail address: dhs@t13.lanl.gov

Department of Applied Mathematics and Statistics, State University of New York at Stony Brook, Stony Brook NY 11794-3600
E-mail address: llwu@ams.sunysb.edu

Department of Applied Mathematics and Statistics, State University of New York at Stony Brook, Stony Brook NY 11794-3600
E-mail address: yan2000@ams.sunysb.edu